ACADEMIC PRESS

Available online at www.sciencedirect.com
SCIENCE DIRECT®

Digital Signal Processing 13 (2003) 1–22

Digital Signal Processing

www.elsevier.com/locate/dsp

Invited paper

Efficient restoration of space-variant blurs from physical optics by sectioning with modified Wiener filtering

Thomas P. Costello [a,*] and Wasfy B. Mikhael [b]

[a] *Mesh Networks, Inc., Maitland, FL 32751, USA*
[b] *Department of Electrical and Computer Engineering, University of Central Florida, Orlando, FL 32826, USA*

Abstract

Digital images blurred by space-variant point-spread functions of uncorrected physical optics may be efficiently restored using Wiener filtering on overlapping subimage frames. Frame size must be tailored to accommodate the displacement-dependent spreading and shifting of physical point-spread functions at large field angles to prevent circular convolution edge effects from corrupting the frame's central section. We define the section as the nonoverlapping subframe used to construct the composite full-image restoration. Otherwise, if the frame is too small, edge-effect errors may extend into the section, inducing artifacts in the composite restoration. Conversely, if the frame is too large, total restoration processing will be greater than necessary. By adjusting frame size with field displacement, we demonstrate the effective restoration of images blurred by a laboratory-grade spherical lens. Blurred images are simulated and then restored with a modified Wiener filter. Mean-square-error and restoration improvement are reported as a function of field angle and criteria are developed for frame and section size selection.

Keywords: Image restoration; Space-variant point-spread function; Physical optics; Sectioning; Wiener filtering

1. Introduction

Restoration of digital images degraded by space-variant (SV) blurs is computationally demanding due to the iterative nature of the specialized restoration methods developed for that purpose. In this work, we propose an efficient noniterative method

* Corresponding author.
E-mail address: tom costello@att.net (T.P. Costello).

1051-2004/02/$ – see front matter
PII: S1051-2004(02)00004-0

for the restoration of space-variant blurs, in particular blurs arising from aberrations in imaging optical systems. The method is based on the sectioning technique [1], but is unique in that restoration-frame size for each section is tailored to the spatial characteristics of the local point-spread function (PSF). The method consists of application of modified Wiener filtering to individual restoration frames that are sized to isolate edge effects from a central subframe used as a nonoverlapping section in the composite restoration.

Several approaches have been reported for the restoration of space-variant image blurs, though most involve narrow application [2–4], extended iteration [5–9] or significant complexity [10–15]. Our proposed method allows efficient, low-complexity restoration of images degraded by a general blur of a physical optical system. To demonstrate the method, we apply it to images with simulated blur from a system composed of a single spherical lens and a square aperture. This is significant because few demonstrations of space-variant image restoration of physical optics blurs have appeared in the literature. Typically, smooth analytical models have been used for blur functions. In this work, we use the diffraction-predicted SV-PSF of the single lens, a laboratory grade spherical biconvex singlet, for the blurring function. As an imaging system, a single spherical lens is severely undercorrected, such that its PSF exhibits significant space-variance and structural complexity even at moderate field angles. But even with sections located at wide field angles, at which Strehl ratios are reduced to less than 5%, we show effective levels of restoration when the frames are appropriately sized.

To determine method parameters, we also conduct three experiments on image sections blurred with the single-lens SV PSF. The experiments demonstrate the efficiency and effectiveness of sectioned Wiener filtering and serve to guide frame size selection as a function of field angle. A two-region approach to full image restoration, as illustrated in Fig. 1, is proposed in which a single large central region, Region 1, is restored with the system's on-axis PSF. Smaller sections in the surrounding Region 2 are restored with local PSFs. Restoration of Region 1 as a single large section is possible due to the general characteristic of near space-invariance of the PSF in the central field-of-view. In the first

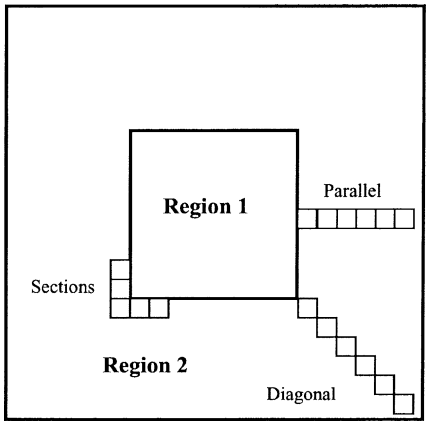

Fig. 1. Two-region approach to full-frame image restoration with sections along parallel and diagonal radii.

experiment, the system's on-axis PSF is used to restore smaller sections blurred with PSFs from a range of field displacements. This establishes worst-case error for the outermost areas of Region 1, which is important because the adjacent sections in Region 2 will have better restoration with the more accurate local PSF. If Region 1 is too large, the abrupt improvement may be noticeable at the boundary of the two regions. The second experiment is conducted similarly, but with local PSFs used for restoration. This experiment establishes the range of displacement over which restoration is effective. The extent of Region 2 for the single-lens system may be defined based on these results. The third experiment varies the size of the restoration frame to reduce edge-ringing errors in Region 2 sections at large field displacements.

The remainder of this paper is organized as follows. Section 2 discusses simulation of the SV image frames used in the experiments, in particular the diffraction-based method for predicting the SV PSF. Section 3 describes the original sectioning technique [7] and our proposed method, which employs modified Wiener filtering [17] over a restoration frame of tailored size. Section 4 describes and gives results of the three experiments we conduct to demonstrate the new method. In Section 5 we give examples of large frame (256×256) restorations at several moderate to wide field displacements and draw conclusions concerning the utility and effectiveness of the restoration method.

2. Space-variant image simulation

In this section, we describe the calculation of the discrete SV blur function of the single-lens optical system and the simulation of the SV digital images used in the experiments. SV image frames are needed at all field locations of interest to conduct the described restoration experiments. We limit our investigation to a maximum displacement of 2^{10} pixels (spaced at the Nyquist sampling period) from the optical axis since the local PSF of the single-lens optical system degrades severely and rapidly beyond that point. Meaningful restoration ($\sim$5 dB) can still be achieved in that range for the single-lens system, but the initial error is so large that the error following restoration is still too large for the section to be useful. We also limit the investigation to sections located along two radii from the optical axis, one parallel and one diagonal to the square system aperture, as illustrated in Fig. 1. PSFs at locations along these radii exhibit structure representative of most image-plane locations. We impose this limitation because the generation of a complete SV image spanning the entire field of interest is a formidable computational task (2^{22} individual PSFs would be required) that is unnecessary since azimuthal PSF variations are only unique over $\pi/4$ radians for a square aperture.

2.1. Image model

A linear deterministic image model with signal-independent AWGN is assumed in simulation of the SV images sections. The model is given by [18]

$$g(x, y) = \int_{\infty}^{\infty}\int_{\infty}^{\infty} h(x, y; \xi, \eta) f(\xi, \eta)\, d\xi\, d\eta + n(x, y), \tag{1}$$

where $g(x, y)$ is the blurred image, $f(\xi, \eta)$ is the undegraded object, $n(x, y)$ is AWGN, and $h(x, y; \xi, \eta)$ is the *incoherent* SV-PSF. Incoherent, quasi-monochromatic illumination is assumed.If $f(\xi, \eta)$ is bandlimited at or below the Nyquist frequency of the image formation system, and the detection system ideally samples at the Nyquist frequency, both of which we assume, then (1) may be discretely approximated by [18]

$$g_{i,j} = \sum_{k=1}^{N} \sum_{l=1}^{N} h_{i,j,k,l} f_{k,l} + n_{i,j}, \quad i, j, k, l = 1, 2, \ldots, N, \tag{2}$$

where $g_{i,j}$ and $f_{k,l}$ are each a square matrix of discrete, uniformly spaced irradiance samples in the image and object planes, respectively, $n_{i,j}$ is a discrete AWGN matrix, and $h_{i,j,k,l}$ is the discrete *incoherent* SV-PSF function describing the irradiance response at image-plane position (i, j) due to a point source at object-plane position (k, l). For the deterministic image model, image restoration is a classical inverse problem of estimating the discrete function $f_{k,l}$ given the discrete functions $g_{i,j}$ and $h_{i,j,k,l}$. In our experiments we simulate $g_{i,j}$ by predicting $h_{i,j,k,l}$ and applying (2) to a known input object $f_{k,l}$.

The period of the N object-plane intervals of (2) is the Nyquist sampling period in the image plane, P_i, projected into object space by the system magnification. P_i is the inverse of the optical system's Nyquist sampling frequency, which is twice the cutoff frequency associated with the $L \times L$ system aperture. The cutoff frequency F_{co}, under the assumption of incoherent illumination, is given by [19]

$$F_{co} = \frac{L}{\lambda d_i}, \tag{3}$$

where λ is the center wavelength of the assumed quasi-monochromatic illumination and d_i is the image distance from the exit pupil. Therefore the image-plane sampling frequency is given by

$$F_N = 2 \cdot F_{co} = \frac{2L}{\lambda d_i} \tag{4}$$

and the period P_i is the inverse of (4) or $P_i = \lambda d_i / 2L$. For a thin lens, the image distance may be approximated as $d_i \cong \text{efl} \cdot (1 - m)$ [20], where efl is the effective focal length and m is the system magnification.

The discrete SV-PSF $h_{i,j,k,l}$ cannot, in general, be obtained by sampling $h(x, y; \xi, \eta)$ since closed-form expressions for physical optics PSFs are generally not available. An approximation of $h(x, y; \xi, \eta)$ from which to sample or a direct approximation of $h_{i,j,k,l}$ is therefore necessary. A method for the latter approach using scalar diffraction theory and the discrete Fourier transform (DFT) is common and will be used here. The following section describes the basic elements of the diffraction-based SV-PSF prediction and the DFT method of discrete approximation.

2.2. Discrete SV-PSF approximation

A SV-PSF function is needed in either continuous or discrete form to simulate SV images and to apply the proposed restoration method. Scalar diffraction theory provides the basis for an approximation of an individual discrete PSF associated with a specific

point-source location. A discrete SV-PSF function may be compiled as the aggregate of individual PSFs, one for each desired discrete image point in the image.

From diffraction theory, the *Fresnel diffraction formula* predicts the complex electric-field amplitude distribution in a plane parallel to a diffracting aperture as a function of the complex field distribution within the aperture and the distance between the planes. The field distribution is assumed to arise from a monochromatic disturbance incident on the aperture. The formula is given in integral form as [19]

$$\mathbf{U}(x_0, y_0) = \frac{1}{j\lambda z} e^{jkz} \iint_{\Sigma} \mathbf{U}(x_1, y_1) \exp\left\{ j \frac{\pi}{\lambda z} \left[(x_0 - x_1)^2 + (y_0 - y_1)^2 \right] \right\} dx_1\, dy_1, \tag{5}$$

where λ is the wavelength of the assumed monochromatic illumination, z is the normal distance separating the aperture and observation planes, $k = 2\pi/\lambda$ is the propagation constant, and Σ represents the physical dimensions of the aperture. The complex amplitude distributions within the aperture and the observation plane are $\mathbf{U}(x_1, y_1)$ and $\mathbf{U}(x_0, y_0)$, respectively.

To use the *Fresnel diffraction formula* to predict a physical PSF, we assume that an ideal plane wave arising from a distant point source is incident on the system entrance pupil. An ideal optical system converts such a plane wave to a convergent and ideally spherical wave in its exit pupil. The wave converges to a point located within the system's image plane and forms an image of the distant point source. We regard the system exit pupil as a diffracting aperture and the convergent spherical wave as its complex amplitude distribution $\mathbf{U}(x_1, y_1)$. If the exit-pupil to image-plane distance is z, then (5) yields the complex amplitude in the image plane, $\mathbf{U}(x_0, y_0)$.

The ideal spherical wave may be defined within the exit pupil as

$$\mathbf{U}_{\Sigma}(x_1, y_1, x_p, y_p) = \frac{A}{R} \exp(-jkR)\, p(x_1, y_1), \tag{6}$$

where (x_p, y_p) is the Gaussian image point of the point source in the image plane, A is the unit radius amplitude of the ideal wave, R is the spherical radius of the wave at exit-pupil point (x_1, y_1), and $p(x_1, y_1)$ is a binary aperture function defined in the exit-pupil plane as unity within the aperture and zero outside the aperture.

With a two-term binomial expansion approximation of the complex exponential radius R in terms of known system parameters, the ideal spherical wave may be expressed as

$$\begin{aligned} \mathbf{U}_{\Sigma}(x_1, y_1, x_p, y_p) = {} & \frac{A}{d_i} p(x_1, y_1) \exp(-jkd_i) \\ & \times \exp\left\{ -j \frac{k}{2d_i} \left[(x_p - x_1)^2 + (y_p - y_1)^2 \right] \right\}, \end{aligned} \tag{7}$$

where d_i is the distance from the exit pupil to the image plane and is used as an approximation of the denominator R term in (6).

In the presence of aberrations, the exit-pupil distribution is not an ideally spherical wave. The actual distribution is a function of the design of the system's optical elements and aperture and the location of the point source in its field-of-view. To describe the effects

of aberrations on the ideal spherical wavefront, a *generalized pupil function* **p** is defined, given by [19]

$$\mathbf{p}(x_1, y_1; x_p, y_p) = p(x_1, y_1) \exp\left(j \frac{2\pi}{\lambda} W(x_1, y_1; x_p, y_p) \right), \tag{8}$$

where $W(x_1, y_1; x_p, y_p)$ is a path-length error function measured along the wave's radius between (x_1, y_1) and (x_p, y_p). Substituting (7) into (5) with $\mathbf{p}(x_1, y_1; x_p, y_p)$ substituted for $p(x_1, y_1)$ yields

$$\mathbf{U}(x_0, y_0; x_p, y_p) = \frac{C}{j\lambda d_i^2} \int_{-\infty}^{+\infty} \int_{-\infty}^{+\infty} \mathbf{p}(x_1, y_1; x_p, y_p) \times \exp\left\{ -j2\pi \left[\frac{(x_0 - x_p)}{\lambda d_i} x_1 + \frac{(y_0 - y_p)}{\lambda d_i} y_1 \right] \right\} dx_1\, dy_1, \tag{9}$$

where $C = \exp\{j(k/2d_i)(x_0^2 - x_p^2 + y_0^2 - y_p^2)\}$ defines a spherical image surface centered on (x_p, y_p).

Equation (9) gives the complex amplitude distribution $\mathbf{U}(x_0, y_0)$ in the image plane arising from a distant monochromatic point source with Gaussian image point (x_p, y_p). The squared modulus of $\mathbf{U}(x_0, y_0)$ is a continuous PSF centered at (x_p, y_p). Also, even though the above derivation is based on strict monochromatic illumination, it can be shown that (9) is valid for quasi-monochromatic illumination with center wavelength $\bar{\lambda}$ under the two conditions that (1) the illumination bandwidth $\Delta\nu$ is small compared to the center frequency $\bar{\nu} = c/\bar{\lambda}$ and (2) $\Delta\nu$ is also much less that c/d_i.

Closed-form solutions of (9) in the presence of aberrations (in which case $\mathbf{p}(x_1, y_1; x_p, y_p)$ is complex) are generally unavailable. In systems composed of spherical surfaces, aberrations are always present, but since (9) has the form of a Fourier transform of $\mathbf{p}(x_1, y_1; x_p, y_p)$ (with spatial frequencies $(x_0 - x_p)/\lambda d_i$ and $(y_0 - y_p)/\lambda d_i$), a discrete sequence approximating samples of $\mathbf{U}(x_0, y_0; x_p, y_p)$ may be obtained by a *discrete Fourier transform* (DFT) of samples of $\mathbf{p}(x_1, y_1; x_p, y_p)$. The transformed sequence samples are an approximation of samples of $\mathbf{U}(x_0, y_0; x_p, y_p)$ because $\mathbf{p}(x_1, y_1; x_p, y_p)$ is space-limited by the physical limits of the aperture and is therefore not bandlimited.

The wave aberration function $W(x_1, y_1; x_p, y_p)$ of the *generalized pupil function* (8) is given by [21]

$$W(x_1, y_1; x_p, y_p) \cong -\frac{1}{4} B r_1^4 - C\kappa^4 - \frac{1}{2} D r_1^2 \rho^2 + E\rho^2\kappa^2 + F r_1^2 \kappa^2, \tag{10}$$

where B, C, D, E, and F are constants whose individual terms in (10) are known as spherical, astigmatism, curvature of field, distortion, and coma aberrations, respectively, or collectively as the *primary* aberrations. Also in (10), $r_1^2 = x_1^2 + y_1^2$ is the exit pupil coordinate radius, $\rho^2 = (x_p^2 + y_p^2)/d_i^2$ is the point-source radius normalized by the object distance, and $\kappa^2 = r_1 \rho \cos\theta$ is the inner (dot) product of the two vectors defined by the scaled point-source radius and the pupil-point radius. The five terms of $W(x_1, y_1; x_p, y_p)$ are the unique combinations, in powers of 4, of the rotational invariants r_1, ρ, and κ. Higher order wave aberration terms are defined, but these fourth order *primary* or *Seidel* terms

describe most low-order optical systems. The Seidel aberration coefficients are specific to the spherical surfaces of the imaging system. The coefficients are a function of the radii of curvature of the surfaces, their axial separation, and the optical index of the lens material. A method for their calculation is given in Ref. [21].

To approximate a PSF at a specific image-plane location (x_p, y_p), the system's Seidel coefficients are determined and the path length error function $W(x_1, y_1; x_p, y_p)$ is substituted into (8). The binary aperture function $p(x_1, y_1)$ in (8) is defined by the physical aperture dimensions. The pupil function $\mathbf{p}(x_1, y_1; x_p, y_p)$ is then sampled on a square uniform grid. A two-dimensional DFT is applied to the resulting sample matrix to generate samples of $\mathbf{U}(x_0, y_0; x_p, y_p)$. The discrete PSF may be obtained by squaring the modulus of each sample. The accuracy of the PSF approximation is determined by the sampling period within the exit pupil. The sampling period of the discrete PSF in the image plane is determined by the spatial extent of the frame over which the exit-pupil plane is sampled. It can be shown that, to obtain Nyquist sampling in the image plane, it is necessary to sample $\mathbf{p}(x_1, y_1; x_p, y_p)$ uniformly over a span twice the dimension of the aperture.

3. Restoration method

Several methods have been reported in the literature for restoration of images degraded by space-variant blurs. Richardson [5] and Lucy [6] each independently developed an iterative maximum likelihood method based on Bayes theorem. It has been widely used, including efforts [23] to restore images from the Hubble Space Telescope prior to its repair. Robbins and Huang [2] demonstrated a method for restoring comatic images assuming no other aberrations were present. Trussel and Hunt [1,7] proposed the sectioning method with a maximum a posteriori (MAP) algorithm. Sawchuck [3] used a coordinate transform method to restore isolated astigmatism aberrations. Angel and Jain used a conjugate gradient method [10]. Schafer et al. [8] developed a very general iterative algorithm that was capable of restoring a variety of degradations, including space-variant blur. Several authors developed set-theoretic methods based on convex projection [11,13,15]. Kalman filtering [12], spatial warping [14], and neural networks [16] have also been demonstrated.

All of these methods have been used to demonstrate impressive restoration results, but they are either restricted by design to a narrowly defined class of systems or their implementations are iterative or very complex. The classical frequency-domain deconvolution methods of inverse-filtering, least-mean-squares (Wiener filtering) and constrained-least-squares are very efficient, but cannot be applied globally in the presence of space-variant blur. Frequency-domain methods may be applied locally to sections of the image over which the blur is nominally constant, but successful restoration of physical optics blurs based on this approach requires additional methodology. This is due to the characteristic spatial spread and shift of physical PSFs at large field angles, which significantly complicates the isolation of edge effects associated with circular convolution. Our proposed method accomplishes edge-effect isolation while maintaining frequency-domain efficiency by combining the sectioning approach, Wiener filtering, and tailored frame sizing.

3.1. Sectioning

The sectioning approach was first proposed [7] for use with the MAP estimation restoration method as an alternative to global Wiener filtering for images obtained with nonlinear sensors and having nonstationary statistics. The authors reported that global Wiener filtering resulted in poor restoration of such images because the method assumes linear system transformation, stationary signal statistics, and stationary, signal independent noise. The authors proposed dividing the image into subimages, or sections, and applying the iterative MAP algorithm locally to individual sections. This allowed iteration truncation to be dependent on local, instead of global, image statistics. Distinct restoration improvement was realized compared to the globally applied Wiener method. Shortly after their initial article on sectioning, the authors reported use of the method to accommodate SV-PSF blurring as well as nonstationary image statistics [1], again using the MAP algorithm under the nonlinear sensor assumption. The method was shown to be capable of addressing the most general image restoration problem, that of the combined degradations of SV-PSF, sensor nonlinearities, and signal-dependent noise.

In addition to the nonstationarity of signal and noise statistics, the primary objection to application of the Wiener filter at the time was sensor nonlinearity since the filter's derivation is based on an assumption of linear system transformation. A number of researchers who accommodated sensor nonlinearity in restoration methods have subsequently concluded that no significant improvement results [22]. In addition, sensor nonlinearity is of most concern with vidicon sensors and scanned photographic film, and we assume modern discrete array sensors, which are regarded as linear. We therefore combine sectioning and Wiener filtering in our approach in order to realize the efficiency and simplicity of frequency domain filtering and impose a relatively small section size to ensure PSF space invariance over the restoration frame.

3.2. Modified Wiener filtering

For linear, space-invariant systems, the classical Wiener filter definition is given by the discrete equation

$$\frac{\hat{F}(u,v)}{G(u,v)} = \frac{H^*(u,v)}{H^*(u,v)H(u,v) + S_n(u,v)/S_f(u,v)}, \tag{11}$$

where $\hat{F}(u,v)$, $G(u,v)$, and $H(u,v)$ are the 2-D DFTs of the discrete object, image, and PSF sample functions $f_{k,l}$, $g_{i,j}$, and h_{i,j,k_0,l_0} of (2) (where k_0, l_0 is the conjugate object point of the section's central pixel), respectively. The object power spectrum term $S_f(u,v)$ corresponds to a class of images, since the derivation of the Wiener filter is based on a statistical model of the image in which the discrete image sample matrix is a single realization of a *random field*. The use of single images to attempt power spectrum estimation of the entire class is problematic and was therefore not attempted here. The noise power spectrum $S_n(u,v)$, although assumed white and known in the SV image simulations of this experiment, is typically unknown in practice as well. For these reasons an empirical constant, termed here a, is substituted for the power-spectra ratio

term $S_n(u,v)/S_f(u,v)$. Thus, the modified Wiener filter used in these experiments is given by [17]

$$\frac{\hat{F}(u,v)}{G(u,v)} = \frac{H^*(u,v)}{H^*(u,v)H(u,v)+a}. \tag{12}$$

The estimate of the restoration frame object spectrum is therefore given by

$$\hat{F}(u,v) = \frac{H^*(u,v)}{H^*(u,v)H(u,v)+a} G(u,v). \tag{13}$$

The final object estimate of the $N \times N$-point restoration frame resulting from the modified Wiener filtering, $\hat{f}_{k,l}$, is given by

$$\hat{f}_{k,l} = \Im_{2D}^{-1}\{\hat{F}(u,v)\}, \quad u,v = 0,1,\ldots,N, \tag{14}$$

where $\Im_{2D}^{-1}\{\}$ is a 2D inverse DFT operation. The discrete image sample spectrum function $G(u,v)$ in (13) is the $N \times N$-point 2D DFT of $g_{i,j}$, where $N \times N$ is the restoration frame size. The Wiener filter function of (13) is also $N \times N$. The object estimate sample function $\hat{f}_{k,l}$ of (14) is correspondingly $N \times N$; however, a band of samples around the function's outer edge is always corrupted by wraparound effects and edge-ringing of the circular convolution represented by (13). The penetration of the corruption from the edge into the estimate's interior is determined by the extent of the Wiener restoration filter in the spatial domain. Thus the usable portion of the object estimate, the section, is a central uncorrupted subframe that is smaller than the restoration frame by the width of the restoration filter.

3.3. Restoration frame sizing

In both Region 1 and Region 2, the modified Wiener filter is applied over a restoration frame that is larger than each nonoverlapping section, but only the section itself is retained for constructing composite full-frame restorations. In general, section size selection is a tradeoff between computational load and restoration error from intrasection PSF space variance. We focus in this investigation on two aspects of full-image restoration, (1) frame size selection, which is a tradeoff between computational load and error from circular convolution edge effects, and (2) the maximum field displacement at which modified Wiener filtering is effective. We therefore select a fixed, moderate section size of 32×32 pixels in Region 2 to mitigate the restoration error contributed by intrasection PSF space variance while maintaining a manageable computational load.

With a fixed section size, the minimum restoration frame size at a given location is determined by the spatial extent of the local Wiener restoration filter. The frame must be at least as wide as the sum of the section size and the width of the filter function to avoid the circular convolution effects of edge oscillation and wraparound data corruption. The Wiener filter has nominally the same extent as its underlying PSF, in terms of encircled energy. At Nyquist sampling, the width of the single-lens system's on-axis PSF is approximately 32×32 pixels (99.5% encircled energy). Therefore, at small to moderate displacement, a 64×64 restoration frame is sufficient for our selected section size to avoid edge-effect corruption within the section.

At moderate displacement, however, space-variant aberrations characteristic of physical PSFs begin to increase the extent of the restoration filter by spreading the PSF energy and radially shifting its centroid. The Wiener restoration filter will exhibit a similar, but compensating, spread and shift. The spread of energy increases wraparound corruption and the shift has the effect of moving any edge oscillation closer to the center of the frame, potentially into the section. Progressively larger frames are therefore necessary as field-displacement increases, beginning at moderate field, to avoid artifacts from edge oscillations and wraparound corruption. We investigate use of frame sizes of 96×96 and 128×128 in our experiments.

Our proposed method of sectioned restoration with Wiener filtering reduces total computation compared to iterative restoration methods while avoiding artifacts arising from characteristics of physical SV-PSFs. The method increases restoration frame size at large displacements, but only as necessary to isolate edge effects. The three experiments described in the next section illustrate these effects and establish field displacement thresholds for increasing frame size for the single-lens optical system.

4. Experiments

This section describes three numerical experiments that illustrate our proposed method for full-frame restoration of images blurred by simple optical systems. In these experiments, we apply the modified Wiener filter to restore image sections blurred by the SV-PSF of the single lens optical system. Five unique blurred sections are restored for each field location of interest over a wide displacement range. Mean-square-error of the five sections following restoration is averaged to characterize expected restoration improvement as a function of field displacement and additive noise level.

The SV-PSF of the single lens system is simulated as described in Section 2. A sufficient number of PSFs is calculated in the neighborhood of each displacement location to generate a blurred image frame four times larger than the desired section to be restored. Sixteen locations are uniformly distributed along each of two radii, one parallel and one diagonal to the aperture edge as illustrated in Fig. 1. For each PSF, the generalized pupil function is sampled on a 64×64 grid over a span of two times the aperture dimension.

The single lens optical system consists of a biconvex, spherical singlet with an effective focal length of 25 mm, a diameter of 25 mm, an on-axis thickness of 10 mm, and an optical index of 1.5. A square aperture is located in a plane coincident with the front apex of the lens and normal to its axis. The aperture is sized to provide an $f/\#$ of 10. Magnification is set at -0.01.

In the first experiment, we restore sections blurred with the single-lens SV-PSF over a range of field displacements using the on-axis PSF and minimum frame size (64×64). This illustrates the diminished restoration performance of global Wiener filtering with an on-axis PSF in a space-variant system. Figures 2 and 3 give the average initial mean-square-error and average restored mean-square-error at each displacement location for five unique SV subimages from the Lena image for parallel and diagonal displacement, respectively. Each figure gives results for four levels of AWGN from 30 to 60 dB. Figures 4 and 5 give

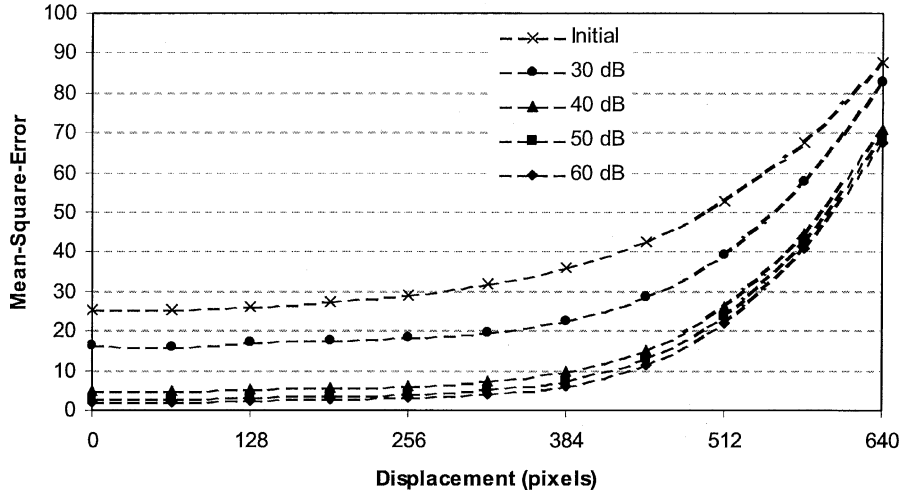

Fig. 2. Mean-square-error in central 32 × 32 section of 64 × 64 restoration frame with modified Wiener method based on on-axis PSF and parallel displacement.

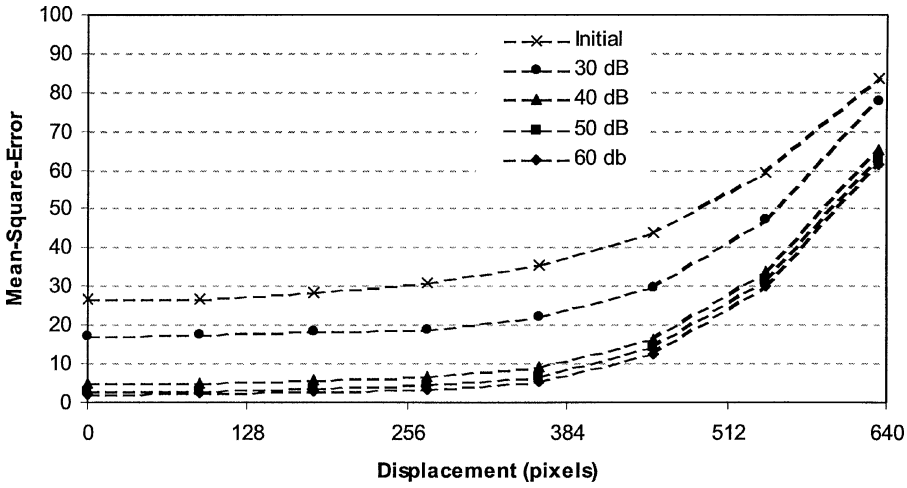

Fig. 3. Mean-square-error in central 32 × 32 section of 64 × 64 restoration frame with modified Wiener method based on on-axis PSF and diagonal displacement.

calculated restoration improvement, based on initial and restored mean-square-error, for the same locations and conditions.

Figures 2 and 3 illustrate the necessity of accommodating a SV-PSF when restoring a SV image. Restored mean-square-error with the on-axis PSF increases dramatically past 384 pixels displacement for both parallel and diagonal displacement. This nominally sets the size of Region 1, which in our method is globally restored with the on-axis PSF. At this size, average MSE at the region boundary would be at most 10 points greater

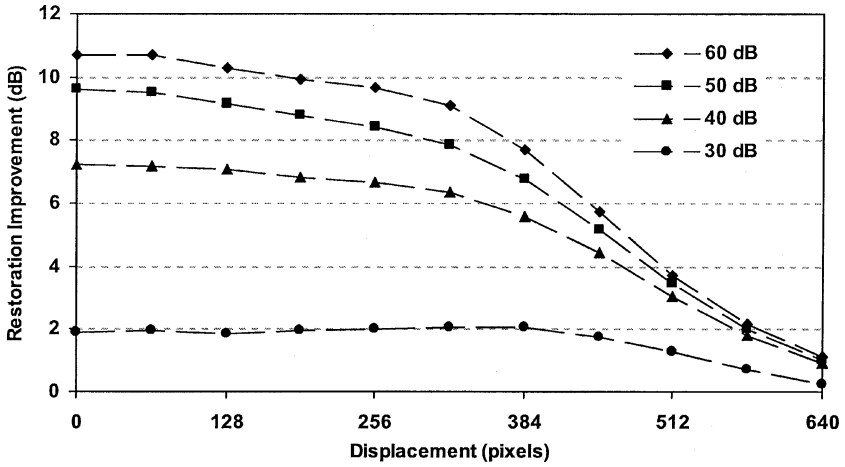

Fig. 4. Restoration improvement in central 32 × 32 section of 64 × 64 restoration frame for modified Wiener method with on-axis PSF for displacement parallel to aperture edge.

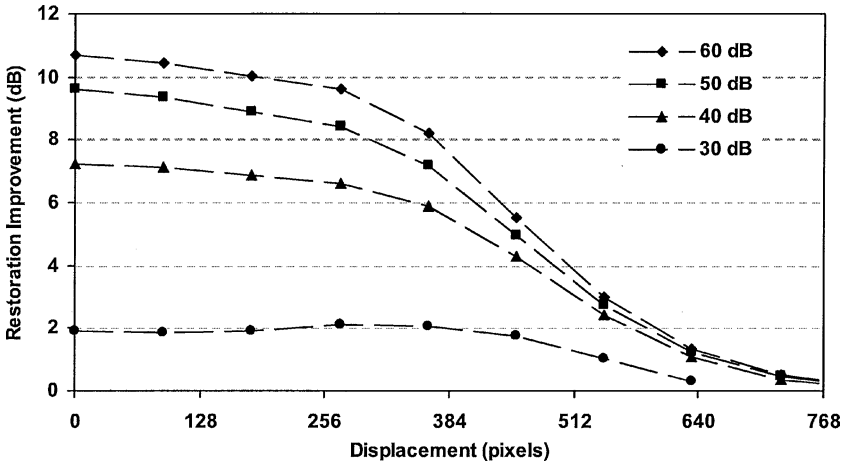

Fig. 5. Restoration improvement in central 32 × 32 section of 64 × 64 restoration frame with modified Wiener method based on on-axis PSF and diagonal displacement.

than restoration with the local PSF. This assumption is verified following the next set of experiments, which provides the local PSF restoration results. A difference in MSE of 10 points across the Region 1–Region 2 boundary is unlikely to induce perceptible artifacts.

The second experiment is identical to the first with the exception that local PSFs are used to restore all sections. The results illustrate the large displacement range over which the modified Wiener filtering is effective. Figures 6 and 7 give average initial mean-square-error and average restored mean-square-error as a function of field angle for parallel and diagonal displacement, respectively. Figures 8 and 9 give the calculated restoration improvement.

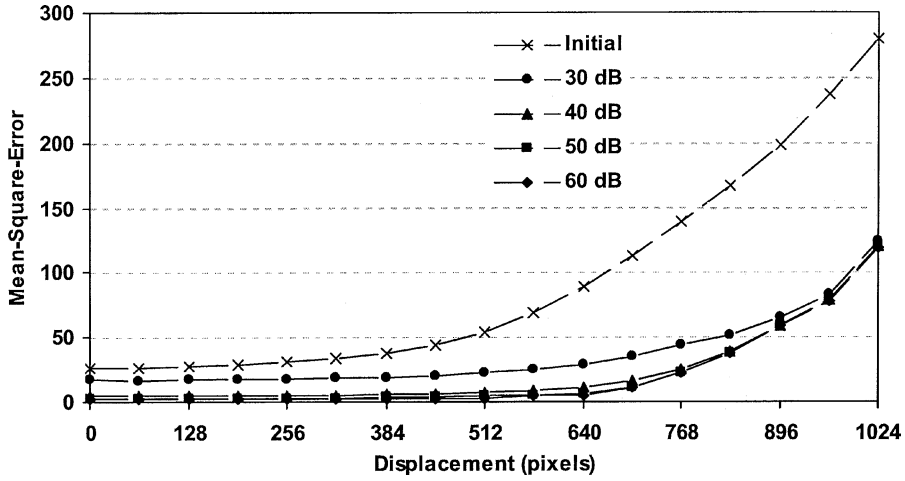

Fig. 6. Mean-square-error for central 32×32 section of 64×64 restoration frame with modified Wiener method for sectioned method with parallel displacement.

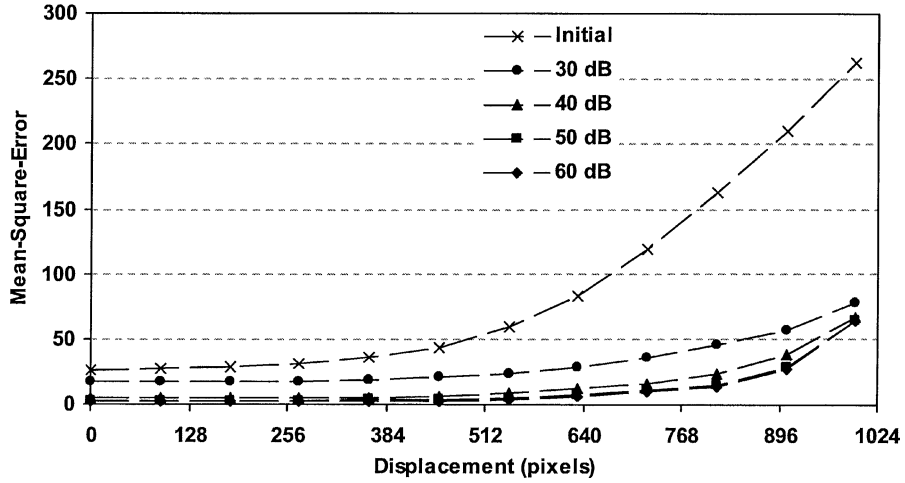

Fig. 7. Mean-square-error for central 32×32 section of 64×64 restoration frame with modified Wiener method for sectioned method with diagonal displacement.

The third experiment compares average restored mean-square-error for local-PSF restoration for the minimum (64×64) and two larger (96×96, 128×128) frame sizes. The very low noise case of 60 dB SNR is used for clarity. As described in the previous section, increasing restoration frame size effectively isolates edge effects magnified by spreading and shifting of the PSF at moderate to large field angles. Figure 10 gives results over the upper half of the displacement range used in the first two experiments since little spreading or shifting of the PSF occurs below that point. The three traces are nearly coincident at the

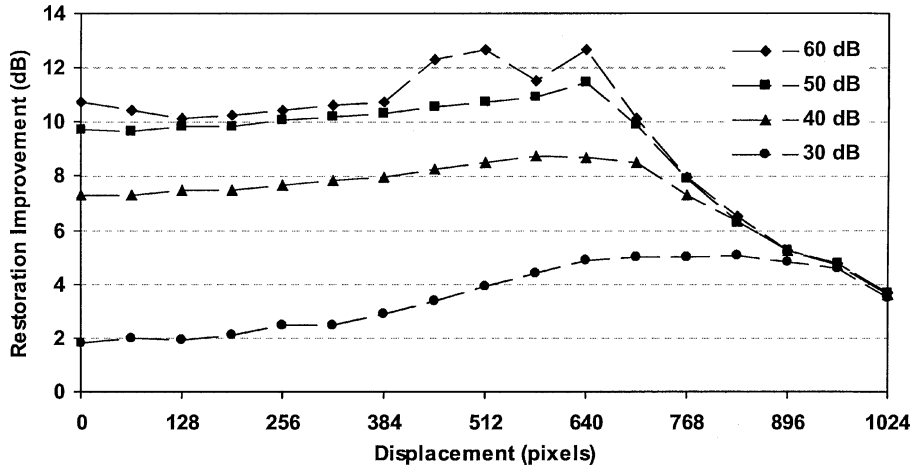

Fig. 8. Restoration improvement over central 32 × 32 section of 64 × 64 restoration frame for modified Wiener method with sectioned approach and parallel displacement.

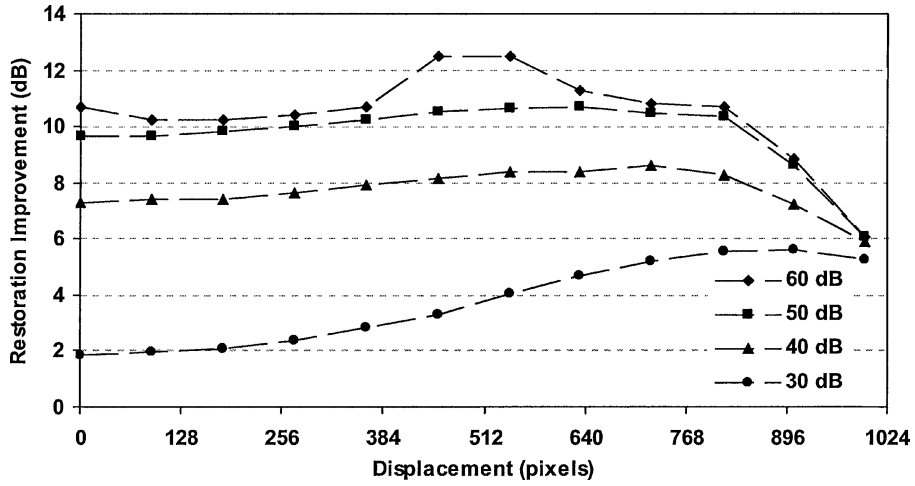

Fig. 9. Restoration improvement over central 32 × 32 section of 64 × 64 restoration frame for modified Wiener method with sectioned approach and diagonal displacement.

lower end of the range, but the trace of the smallest (64 × 64) frame begins to diverge at about 896 pixels total displacement. Restoration benefits significantly in this range from an intermediate size (96 × 96) frame. A specific example is given in the next section. The trace of the intermediate frame begins to diverge from the trace of the largest (128 × 128) frame at about 1000 pixels total displacement, suggesting the larger frame is necessary beyond that displacement. An example in this displacement range is given in the next section as well.

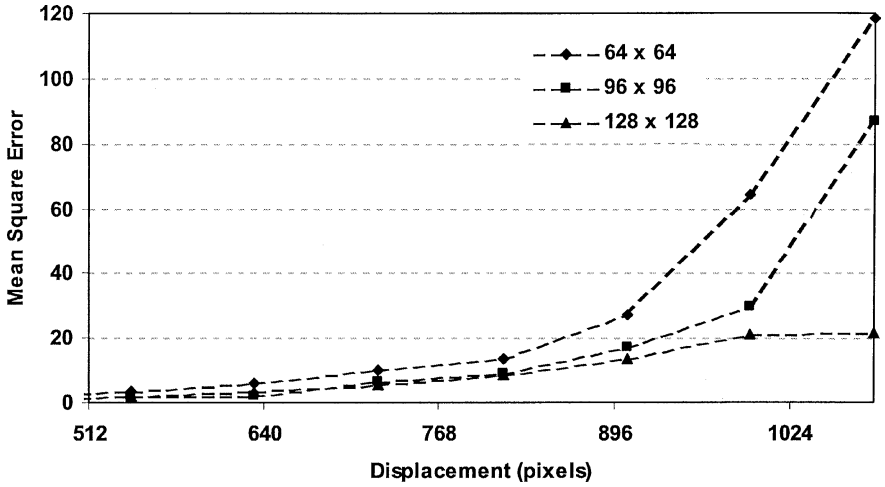

Fig. 10. Mean-square-error for 32 × 32 sections, diagonally displaced, following modified Wiener filtering restoration with 3 frame sizes.

5. Restoration examples

Three restoration examples that demonstrate the proposed method are given in this section. In each example a 256 × 256 image blurred with the single-lens SV-PSF of Section 4 is restored with modified Wiener filtering applied to 32 × 32 sections. The first example, presented in Figs. 11–14, shows restoration of the image blurred at 512 × 512 pixels displacement and illustrates the benefit of the sectioning approach even at moderate field angle. Figure 11 is the blurred image. Figure 12 shows the results of global restoration of the image by Wiener filtering with the on-axis PSF, which yields little improvement in MSE. Global Wiener restoration with the local PSF, shown in Fig. 13, does result in significant restoration improvement of greater than 5 dB. Sectioned restoration with the modified Wiener filter and a 64 × 64 frame size, shown in Fig. 14, accomplishes visibly better improvement of greater than 10 dB.

The second example illustrates the effect of increasing restoration frame size once edge effects begin to corrupt sections at larger field displacement. Figure 15 shows the image blurred at 640 × 640 pixels displacement. Figure 16 is sectioned restoration with the modified Wiener filter with a 64 × 64 frame. Progressively prominent edge artifacts are visible in individual sections at larger displacements (matrix format coordinates are used with increasing displacement from left to right and top to bottom). Figure 17 is the same restoration with a 96 × 96 frame. Few edge artifacts are noticeable and mean-square-error is reduced by nearly a factor of 2.

The third example illustrates the same effect at an even larger displacement. Figure 18 shows the image blurred at 768 × 768 pixels displacement. Sectioned restoration with the modified Wiener filter with a 96 × 96 frame, shown in Fig. 19, exhibits significant edge artifacts. The same restoration with a 128 × 128 frame, shown in Fig. 20, exhibits very few artifacts and an improved mean-square-error.

Fig. 11. Lena image blurred with SV PSF at 512×512 (724 total) field displacement. MSE is 189.

Fig. 12. Global Wiener restoration of Fig. 11 with on-axis PSF. MSE is 169 and improvement is 0.5 dB.

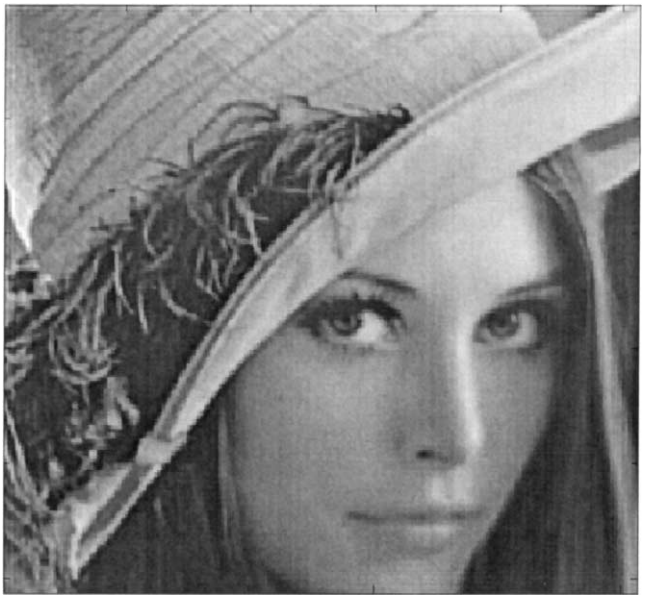

Fig. 13. Global Wiener restoration of Fig. 11 with local PSF at 512 × 512 (724 total) field displacement. MSE is 55 and improvement is 5.4 dB.

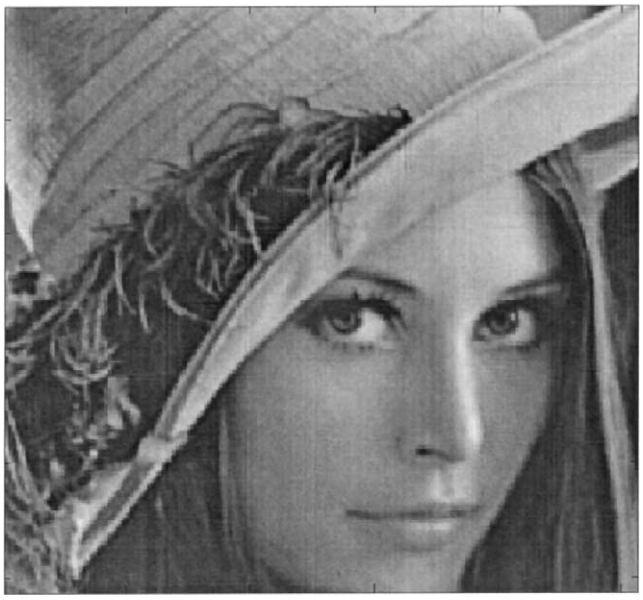

Fig. 14. Sectioned Wiener restoration of Fig. 11 with 64 × 64 frame size. MSE is 15 and improvement is 10.7 dB.

Fig. 15. Lena image 256 × 256 blurred with SV PSF at 640 × 640 (905 total) field displacement. MSE is 317.

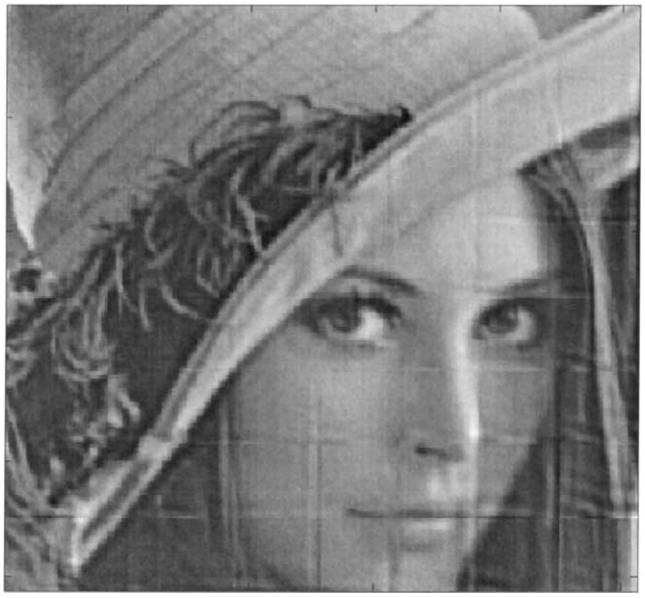

Fig. 16. Sectioned Wiener restoration of Fig. 15 with 64 × 64 frame size. MSE is 65 and improvement is 6.9 dB.

Fig. 17. Sectioned Wiener restoration of Fig. 15 with 96 × 96 frame size. MSE is 38 and improvement is 9.2 dB.

Fig. 18. Lena image 256 × 256 blurred with SV PSF at 768 × 768 (1086 total) field displacement. MSE is 470.

Fig. 19. Sectioned Wiener restoration of Fig. 18 with 96×96 frame size. MSE is 214 and improvement is 3.4 dB.

Fig. 20. Sectioned Wiener restoration of Fig. 18 with 128×128 frame size. MSE is 69 and improvement is 8.4 dB.

6. Conclusions

We propose an efficient restoration method for images blurred by the space-variant PSF of simple physical optical systems. We demonstrate the method by restoring sections of images with SV blur over a wide range of field displacement. It is assumed the image has sufficiently wide field-of-view to incur significant SV blurring from optical aberrations. The method consists of dividing the image into two regions, a central section covering nominally one third to one half of the field-of-view and the remaining outer section. The central section, Region 1, is restored as a single section by global modified Wiener filtering to take advantage of the small degree of PSF space-variance near the optical axis. The outer section, Region 2, is restored with the sectioning method and modified Wiener filtering to accommodate progressively increasing space-variance with displacement. Edge-corruption effects associated with frequency-domain filtering are seen to be aggravated by PSF spreading and shifting, which is characteristic in physical optics at moderate to large field angles. We demonstrate effective mitigation of these effects by increasing restoration frame size at larger field displacements.

References

[1] H.J. Trussel, B.R. Hunt, Image restoration of space-variant blurs by sectioned methods, IEEE Trans. Acoustics, Speech Signal Process. 26 (1978) 608–609.
[2] G.M. Robbins, T.S. Huang, Inverse filtering for linear shift-variant imaging systems, Proc. IEEE 60 (1972) 862–872.
[3] A.A. Sawchuck, Space-variant image restoration by coordinate transformation, J. Opt. Soc. Am. 64 (1974) 138–144.
[4] A.A. Sawchuck, M.J. Peyrovian, Restoration of astigmatism and curvature of field, J. Opt. Soc. Am. 65 (1975) 712–715.
[5] W.H. Richardson, Bayesian-based iterative method of image restoration, J. Opt. Soc. Am. 62 (1972) 55–59.
[6] L.B. Lucy, An iterative technique for the rectification of observed disturbances, Astron. J. 79 (1974) 745–754.
[7] H.J. Trussel, B.R. Hunt, Sectioned methods for image restoration, IEEE Trans. Acoustics, Speech Signal Process 26 (1978) 157–164.
[8] R.W. Schafer, R.M. Mersereau, M.A. Richards, Constrained iterative restoration algorithms, Proc. IEEE 69 (1981) 432–450.
[9] T.P. Costello, W.B. Mikhael, Restoration of digital images with known space-variant blurs from conventional optical systems, Proc. SPIE (Visual Information Processing VIII) 3716 (1999) 71–79.
[10] E.S. Angel, A.K. Jain, Restoration of images degraded by spatially varying point spread functions by a conjugate gradient method, Appl. Opt. 17 (1978) 2186–2190.
[11] M.I. Sezan, H. Stark, Image restoration by convex projections in the presence of noise, Appl. Opt. 22 (1983) 2781–2789.
[12] A.M. Tekalp, G. Pavlovic, Space-variant and color image restoration using Kalman filtering, in: Proceedings of the IEEE International Symposium on Circuits and Systems, 1989, pp. 9–12.
[13] M.I. Sezan, A.M. Tekalp, Adaptive image restoration with artifact suppression using the theory of convex projections, IEEE Trans. Acoustics, Speech Signal Process. 38 (1990) 181–185.
[14] S.R. McNown, B.R. Hunt, Approximate shift-invariance by warping shift-variant systems, Proc. SPIE (Image Reconstruction and Restoration) 2302 (1994) 156–167.
[15] M.K. Ozkan, A.M. Tekalp, M.I. Sezan, POCS-based restoration of space-varying blurred images, IEEE Trans. Image Process. 3 (1994) 450–454.

[16] S.W. Perry, L. Quan, Neural network restoration of images suffering space-variant distortion, Electr. Lett. 31 (1995) 1358–1359.
[17] B. Gonzales, R. Woods, Digital Image Processing, Addison–Wesley, New York, 1993.
[18] K.C. Andrews, B.R. Hunt, Digital Image Restoration, Prentice–Hall, Englewood Cliffs, NJ, 1977.
[19] J. Goodman, Introduction to Fourier Optics, McGraw–Hill, New York, 1968.
[20] W.J. Smith, Modern Optical Engineering, McGraw–Hill, New York, 1990.
[21] M. Born, E. Wolf, Principles of Optics, Pergamon Press, New York, 1980.
[22] A.K. Katsaggelos (Ed.), Digital Image Restoration, Springer-Verlag, New York, 1991.
[23] A.F. Boden, D.C. Redding, R.J. Hanisch, J. Mo, Massively parallel spatially variant maximum likelihood restoration of Hubble Space Telescope imagery, J. Opt. Soc. Am. A 13 (1996) 1537–1545.

Thomas P. Costello is a staff engineer at Mesh Networks, Inc. in Maitland, Florida, working on simulation of spread-spectrum RF modems for mobile IP networking and VoIP architecture for handheld computers. He holds a Ph.D. and M.S. in electrical engineering from the University of Central Florida (2001 and 1992, respectively) and a B.S. in mechanical engineering from the University of Florida (1982).

Wasfy B. Mikhael is a professor in the School of Electrical Engineering and Computer Science of the University of Central Florida, Orlando, Florida. He is Vice President for regions 1–7 in the IEEE Circuits and Systems Society and is a Fellow of the IEEE (1987) for contributions to the development of hybrid and integrated filtering circuits and systems. He received the B.Sc. (honors) in electronics and communications from Assiut University, Egypt, the M.Sc. EE from the University of Calgary, Calgary, Alberta, Canada, and the D. Eng. from Sir George Williams University, Montreal, Canada, in 1965, 1970, and 1973, respectively. His research and teaching interests are in analog, digital, and adaptive digital signal processing of one and multidimensional signals and systems, with applications.